International Journal of Mechanical Engineering and Technology (IJMET)
Volume 9, Issue 9, September 2018, pp. 1463–1474, Article ID: IJMET_09_09_160
Available online at http://www.iaeme.com/ijmet/issues.asp?JType=IJMET&VType=9&IType=9
ISSN Print: 0976-6340 and ISSN Online: 0976-6359

STUDY THE POSSIBILITY OF IMPROVING INDUCTION HEATING OF FDM 3D PRINTER NOZZLE

I.I. Bezukladnikov, D.N. Trushnikov, Yu.A. Shilova, A.A. Yuzhakov, A.A. Oskolkov, E.V. Matveev

Perm National Research Polytechnic University, Perm, Russia Federation

ABSTRACT

This article describes the FDM technology of 3D printing. Among the list of problems of FDM technology highlighted in the article, the so-called human factor stands apart. The authors found one of the possible solutions to minimize this harmful factor and others. The solution is to create a method for managing the printing process, on multiparametric dynamic-response control over various parameters directly in the process of printing. This article is devoted to improving technology, providing fast and accurate temperature control directly in the process of printing. Such a technology is the induction heating of a nozzle. The main attention is paid to the disadvantages of the method of induction heating of a nozzle, namely its uneven. This article covers the issues related to optimization of the induction heating in order to improve its evenness. A system of induction heating, basic physical processes and a mathematical model of this system are described. The electromagnetic and thermal tasks are set within one multi-physical mathematical model of the previously described system. The corresponding parametric task with such a variable parameter as heating frequency was numerically solved using Comsol Multiphysics modelling environment. Based on the obtained data, the inductor physical design was changed and the previous parametric task was solved once again. On the basis of the obtained results, it was concluded that the completed optimization practically linearise the temperature curve for the major part of the area characterized by active heating of the nozzle. To confirm this hypothesis, a test stand was designed, the results of printing on which fully confirmed the data of mathematical modeling and ensured a significant increase in printing quality.

Key words: Additive Manufacturing, FDM, 3D Printing, Induction Heating, Electromagnetic Induction, Uneven Heating, Mathematical Modeling, Multiparametric Control, Dynamic-Response Control, Temperature Control, Resistive Heating, Electromagnetic Oscillation, Inductor, Printing Quality.

Cite this Article: I.I. Bezukladnikov, D.N. Trushnikov, Yu.A. Shilova, A.A. Yuzhakov, A.A. Oskolkov, E.V. Matveev, Study the Possibility of Improving Induction Heating of FDM 3D Printer Nozzle, *International Journal of Mechanical Engineering and Technology* 9(9), 2018, pp. 1463–1474.
http://www.iaeme.com/IJMET/issues.asp?JType=IJMET&VType=9&IType=9

1. INTRODUCTION

Presently, 3D technologies affect an increasing number of human life areas. Thus, in addition to architecture, construction, and aviation, 3D printers find their application in clothes manufacturing and even in some food production. The printers can be classified into several groups depending on the size of the item, printing technology, material used for the production, and scope of application. Fused Deposition Modelling (FDM) is one of the groups. Such printing results in extruding some material through an extrusion nozzle. In the case when the input material is solid, the FDM technology preliminary changes the aggregative state of the material (melts it). The nozzle through which the material is extruded is heated for this purpose. Most of desk-top FDM printers employ resistive heating [1, 2]. In this case, the main disadvantages found in FDM/FFF 3D printing are related to its most vulnerable parts: extruder and nozzle. These are big thermal mass of the heated part, low heating temperature, low heating gradient, low throughput capacity, high vibration rate, limitations on the trolley speed rate, and low precision of the positioning. Another problematic aspect of any 3D printing is the human factor or a 'link' between the printer and a 3D model of a future product. Notwithstanding the widespread application of 3D printers and numerous manuals available free of charge, it is rather difficult to print an ideal product from the first time having no expertise. A possible alternative can be an approach based on multiparametric dynamic-response control over various parameters directly in the process of printing. In this case, the induction heating of a nozzle—a working part of the extruder-proves to be perspective. The induction heating is a non-contact heating method [3, 4], which allows heating the exact pre-set part of a conduit to a high temperature within a short period of time. This allows to significantly reduce thermal mass of the extruder as well as to eliminate the necessity to apply numerous heat insulations that impact the operating temperature range and other quality parameters. The known prototypes of an induction extruder [5] showed higher operational properties compared to the known resistance-based options (having operating temperature up to 1000 °C, possibility to use all-metal nozzles made of solid materials, possibility of automatic removal and cold replacement of a nozzle during the printing process, etc.) [6, 7]. However, despite the obvious advantages, the available solutions have several drawbacks, the most significant of which is uneven nozzle induction heating. This article covers the issues related to optimization of the induction heating in order to improve its evenness.

2. MODELLING PROBLEM SETTING AND GENERAL DESCRIPTION OF PHYSICAL PROCESSES

An induction system for heating the nozzle in the FDM 3D printer contains the following: 1) a high frequency semiconductor source assembled according to the full bridge diagram (Fig. 1) with controlled phase shift, 24V power voltage, power capacity up to 300W, frequency from 5 to 500 kHz; 2) a frameless inductor of a specified diameter and height, consisting of 20 coils of copper high-frequency wires (litz wire); 3) a magnetic flux concentrator made of iron-filled polymer composite in the form of external cylindrical shell of the inductor; 4) an aluminium cylindrical mandrel that functions as shield against the high frequency magnetic field and as mechanical fastening of the heater to the extruder frame; 5) a working body (Fig. 2, left to

right), which is the nozzle for FDM 3D printing of a preset configuration made of ferromagnetic alloy 40 x 13 with an inductor inside channel of 2 mm diameter and 0.4 mm opening. It is worth noting that the physical design of the inductor, concentrator, and other elements in the system is close to axially symmetrical one, which gives the opportunity to consider the induction heating system as a two-dimensional model, to use cylindrical coordinate system (0rz), and, therefore, to significantly simplify the process of modelling. Below we consider mathematical models of fundamental physical processes occurring in the system described when the nozzle is heated [8, 9, 10, 11].

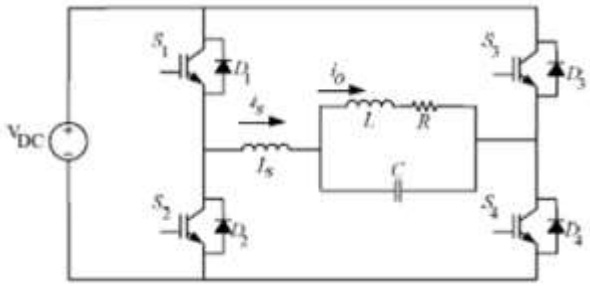

Figure 1 Simplified circuit diagram of the induction heating power source

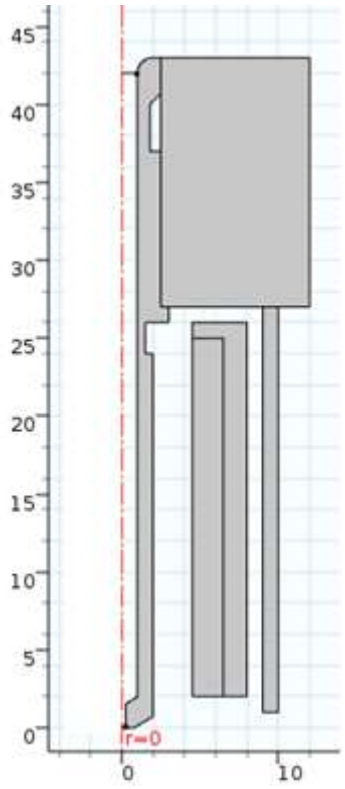

Figure 2 Drawing of the induction heating system for FDM 3D nozzle

Electromagnetic Task. To simplify the modelling, we assume that the load of the power source (inductor) is consistent, the oscillation frequency is adjusted automatically, and accordingly, at any specific time, the harmonic current ***I*** of the known value flows in the inductor coil. In this case, the electromagnetic processes existing in such a system are described by the following system of differential equations in relation to a single-component complex magnetic vector potential $\dot{A}_\varphi : \dot{\mathbf{A}} = (0, \dot{A}_\varphi, 0)$.

For the space area occupied by the working body:

$$j\omega\sigma\dot{\mathbf{A}}+\nabla\times(\mu_0^{-1}\nabla\times\dot{\mathbf{A}})=0; \tag{1}$$

For the space area containing the i*th* inductor coil:

$$\begin{gathered} j\omega\sigma\dot{\mathbf{A}}+\nabla\times(\mu_0^{-1}\nabla\times\dot{\mathbf{A}})=\sigma\dot{U}_i/(2\pi r), \\ \dot{U}_i=\frac{\dot{I}+\int\limits_{S_i} j\omega\sigma\,\dot{A}_\varphi dS_i}{\sigma\int\limits_{S_i}1/(2\pi r)\,dS_i}, \\ \dot{J}_\varphi=-j\omega\sigma\,\dot{A}_\varphi+\sigma\dot{U}_k/(2\pi r); \end{gathered} \tag{2}$$

For the space area occupied by the magnetic flux concentrator

$$\begin{gathered} j\omega\sigma\dot{\mathbf{A}}+\nabla\times(\mu_0^{-1}\nabla\times\dot{\mathbf{A}})=\sigma\dot{U}_k/(2\pi r), \\ \dot{U}_k=\frac{\int\limits_{S_k} j\omega\sigma\,\dot{A}_\varphi dS_k}{\sigma\int\limits_{S_k}1/(2\pi r)\,dS_k},\quad \dot{I}=\int\limits_{S_i}\dot{J}_\varphi dS=0, \\ \dot{J}_\varphi=-j\omega\sigma\,\dot{A}_\varphi+\sigma\dot{U}_k/(2\pi r); \end{gathered} \tag{3}$$

For ambient air

$$\nabla\times(\mu_0^{-1}\nabla\times\dot{\mathbf{A}})=0. \tag{4}$$

In all the equations above: σ—the electric conductivity of the material (alloy 40 x 13, copper, concentrator made of iron-filled polymer composite, air); ω—angular frequency; *j*—unit imaginary number; μ_0 and ε_0—magnetic and electrical permittivity of vacuum correspondingly; $\mu_0=1.256*10^{-6}$, $\varepsilon_0=8.85*10^{-12}$ F/m; J_φ—current density in the inductor; r—radial coordinate; S_i – cross sectional area of the inductor; S_k—cross sectional area of the concentrator; U_i—originally unknown voltage drop at the i*th* inductor coil; U_k—induced voltage drop in the concentrator; ***I***—electric current flowing in inductor coils (set value).

Full voltage value ($\boldsymbol{U}_н$) across the inductor is defined as the algebraic sum of voltages defined in all the coils. The value of this voltage is used in calculation of active and reactive power consumed by the system. Frequency-related equivalent complex impedance in such a system is defined as follows $\dot{Z}=\dot{U}_н/\dot{I}$.

Boundary conditions of the task described by (1)-(4) system can be considered a condition of symmetry about the z-axis and magnetic insulation at the external boundaries of the computational domain $\dot{A}_\varphi=0$.

Thermal Task. The inductor and the concentrator in the system under consideration are cooled due to thermal contact with the external cylindrical mandrel, which operates as a housing, and is mechanically connected to the extruder radiator that is equipped with forced

ventilation. To simplify the task, we assume that the thermal contacts are ideal and the extruder cooling is enough to provide for the cooling of the inductor and the concentrator. Accordingly, the temperature throughout them is constant and does not exceed the value of T = 50°C. Subject to this admission, the mathematical model of non-stationary thermal process of a workpiece induction heating can be described by only 2 equations [9, 12]:

$$\rho C_p \frac{\partial T}{\partial t} - \nabla\lambda\nabla T = \begin{cases} Q & \text{in the area of the heated nozzle,} \\ 0 & \text{in other areas of the model} \end{cases} \quad (5)$$

Here p=p(T), $C_p=C_p(T)$, λ = λ(T) is the density, specific heat capacity and thermal conductivity of the material in the corresponding environment depending on temperature T (respectively); Q—specific capacity of the heat source that provides for the induction heating of the working area with whirling currents,

$$Q = \frac{\dot{j}\,\dot{j}^*}{\sigma} = \omega^2\sigma(\dot{A}_\varphi \dot{A}_\varphi^*), \qquad J = -j\omega\sigma A_\varphi \quad (6)$$

where J is the working value of the induced current density within the ferromagnetic nozzle; A_φ *is* a complex conjugate of the magnetic potential. Heat transfer in the form of convection and radiation in the system can be neglected due to the small contribution made by these mechanisms compared to the heat transfer in the result of the thermal conductivity of materials.

For this task, the boundary conditions can be accepted as the Neumann condition dT/dr = 0 on the axis of symmetry. In the area of the inductor and the concentrator having the forced cooling, we take T = const = 50 °C. At the external boundaries of the computational domain, we set the condition of heat exchange with the environment $-\lambda\partial T/\partial\mathbf{n} = k(T - T_0)$, where k is the coefficient of heat transfer; T_0 is the environment temperature, **n** is an outward normal vector to the boundary.

To view these tasks in the Comsol Multiphysics interface we can use standard physical interfaces: Magnetic Fields (mf) and Heat Transfer in Solids (ht). Both tasks can be solved simultaneously within one multi-physical model due to their connection to each other through Joule heat determined by formula (6). The input data for the modelling are shown in the table below

Table 1 Input data of a multi-physical model

Inductor	
material	copper: electrical conductivity—$5.998*10^7$ S/m relative magnetic permittivity—1 relative electrical permittivity—1
number of coils	20
inner diameter, mm	9
outer diameter, mm	13
height, mm	23
power source voltage, V	24
oscillation frequency, kHz	5..150
current, A	15
Magnetic flux concentrator	

material	iron-filled polymer composite: basis is heat-conducting insulating silicone compound KPTD-1-5 filler is ferrous powder electrical conductivity – 0.004 S/m relative magnetic permittivity—200 relative electrical permittivity—3.6
inner diameter, mm	13
outer diameter, mm	15
height, mm	24
Cylindrical mandrel, extruder housing	
material	aluminium: electrical conductivity – $3.774*10^7$ S/m relative magnetic permittivity—1 relative electrical permittivity—1
inner diameter, mm	15
outer diameter, mm	17
height, mm	30
Working body (nozzle) of the extruder	
material	steel 40 x 13 electrical conductivity – $1.12*10^7$ S/m relative magnetic permittivity—380 relative electrical permittivity—1
height of the active part, mm	22
inner diameter, mm	2
outer diameter of the active part, mm	4
output opening diameter, mm	0.4
outer diameter of a thermal barrier, mm	3
height of a thermal barrier, mm	2
outer diameter of a nozzle shank, mm	6
height of a nozzle shank, mm	30
Additional data for thermal task solution	
Input environment temperature	20 °C
coefficient of heat transfer, W/(m^2/K)	15

Initial conditions make the following equations $\dot{A}_\varphi|_{t=0}=0,\ T|_{t=0}=T_0,\ \mathbf{v}|_{t=0}=0,\ p|_{t=0}=0$.

Numerical implementation is carried out using finite-elements method in Comsol Multiphysics 4.3 applied software package. According to the multi-physical task classification shown in [2], [7], the connection between the listed tasks is weak, and they can be solved sequentially. In this case, the electromagnetic task is to be solved first; the solution shall be further used to solve the thermal task [13, 14].

The results of numerical modelling of physical processes at f = 19.5 kHz (this is the current operating frequency of the induction extruder prototype), t = 4 s, are listed below:

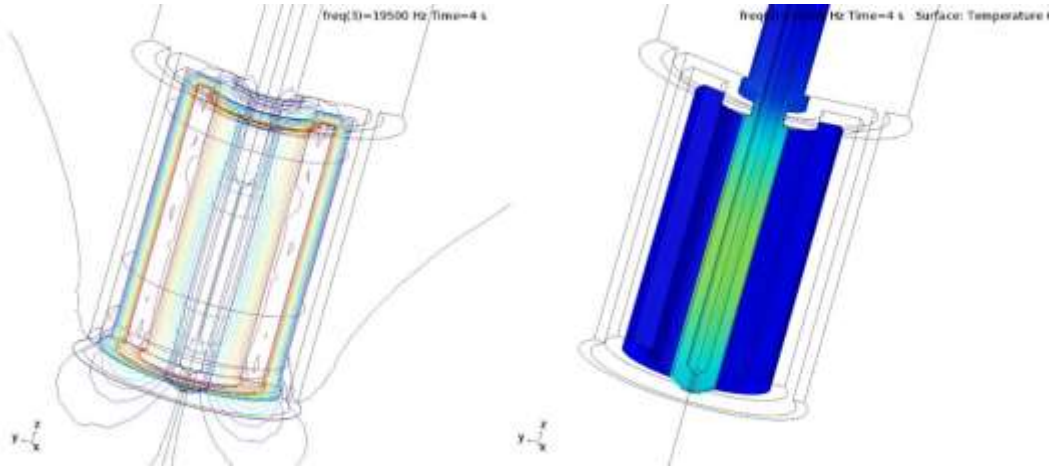

Figure 3 Results of the electromagnetic and thermal tasks at f = 19.5 kHz, t = 4 s

As it can be seen on the left side of the Figure, at the selected frequency, the penetration depth of the electromagnetic radiation is significantly bigger in the endings of the nozzle working zone than in its middle part. This reduces the electrical resistance in relevant sections of the working zone, and, consequently, reduces the dissipated power (useful heating). The Figure on the right shows the temperature map of the extruder nozzle heating at t = 4, which reflects the described situation. More accurate temperature distribution in various sections of the heated nozzle can be seen in Fig. 4, which is a graph of temperature distribution for the vertical section (coordinate r = 1.15 mm). The left diagram of the relevant part of the nozzle in a scale is given to facilitate understanding of the graph.

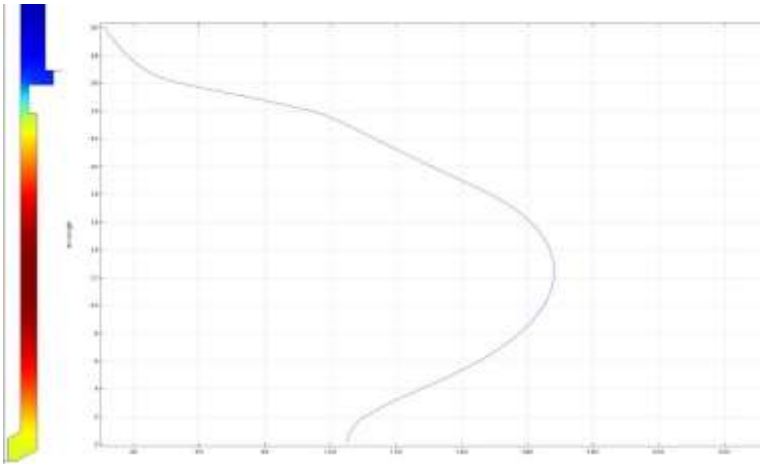

Figure 4 Temperature distribution in heated nozzle at t = 4 s, section r = 1.15 mm

In the given figure, the temperature difference in the central part of the heated nozzle is 76 degrees compared to the periphery (92 degrees for the point on z = 24, 168 degrees for the point on z = 12.2). Such a significant unevenness leads to local overheating of the fed material. In the case when the fed material is different polymers with high thermal expansion rates, it leads to increased pressure in the nozzle and uncontrolled efflux of a certain amount of plastic from the work opening. This effect is found in most of the FDM 3D printers existing on the market and significantly degrades the quality of a 3D-printed item (Fig. 5).

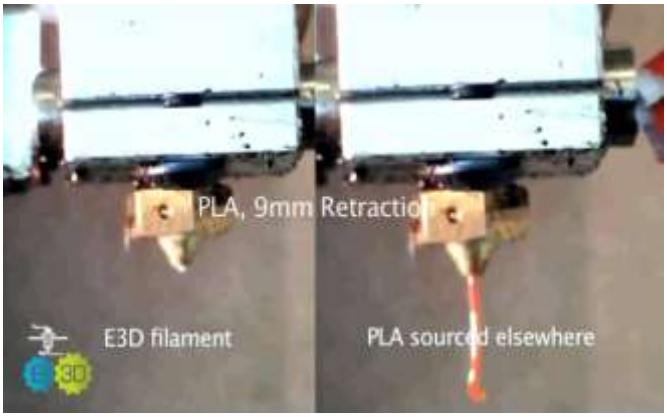

Figure 5 Uncontrolled efflux of plastic due to local overheating of hot parts in extruder (photo by https://e3d-online.com/)

In addition, it should be noted that one of the main parameters affecting the quality of printing is a temperature gradient in the thermal barrier zone (Fig. 2, z = 24 ... 26 mm). The temperature difference in this area must be enough to rapidly reach the glass transition point. In this case, the plastic fed from above functions as a piston pushing the underneath melt towards the work opening. The most high-quality printing is achieved at an ultimately rapid temperature change (minimum height of the formed plug). For the temperature pattern observed in Fig. 4, the height of the corresponding zone is about 10 mm, which is insufficient for printing with a large nomenclature of plastics (Flex, Rubber, Soft, etc.).

Since the main reason of the disadvantages listed above is uneven heating of the working zone of the nozzle caused by uneven penetration of electromagnetic oscillation during the induction heating, it was decided to optimize the heating frequency since this parameter directly affects both the depth of penetration and the overall distribution of electromagnetic oscillation in the inductor. The corresponding parametric task with such a variable parameter as heating frequency was numerically solved using Comsol Multiphysics modelling environment for the whole operating range of the source frequency (5 ... 150 kHz) with a parameter step of 7.25 kHz. To save the space, the following consolidated graph shows the temperature distribution lines similar to those shown in Fig. 4.

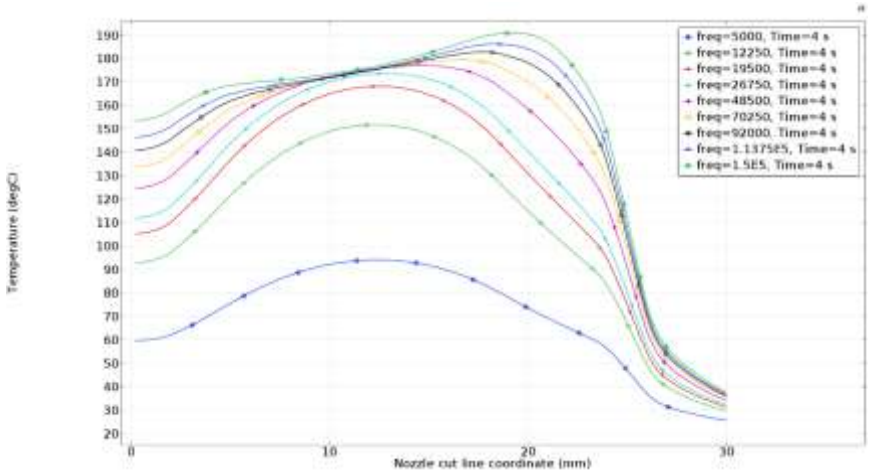

Figure 6 Solution of thermal part of the parametric multi-physical task for f = 5.. 150 kHz

As shown in the Figure, 6 kHz frequency is not efficient for heating the nozzle of required configuration due to the extremely small diameter (the heating efficiency is less than 50%). The significant growth in the heating efficiency is observed up to the frequency of f = 26750

kHz, beyond which the changes mainly relate to the temperature distribution along the length of the nozzle. The frequencies ranging from 92 to 150 kHz are characterized by practically monotonously increasing temperatures over the major part of the working area (from z = 3 to z = 21 mm) with a growing inclination of the relevant parameter.

To eliminate the unwanted parameter inclination, an additional stage of modelling was completed for a changed physical design of the inductor. Given the observed heating curve shape, it was decided to change an inclination of the coiling base at the stage of inductor winding (after such a modification the inductor will have the form of a truncated hollow cone, rather than of a hollow cylinder). In terms of models, it is reflected in inclination of the corresponding geometric components. To reflect the modifications, an additional parametric multi-physical task was created and resolved in relation to parameter α—the angle of the coiling base in the inductor relative to the z-axis. After an optimal slope angle value $\alpha = 1^{o}$ for the obtained system configuration has been determined, the previous parametric task was solved again at f = 34.. 150 kHz.

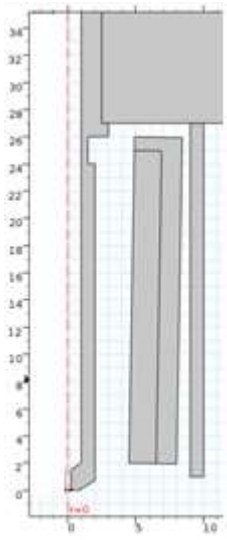

Figure 7 Modified form of the inductor

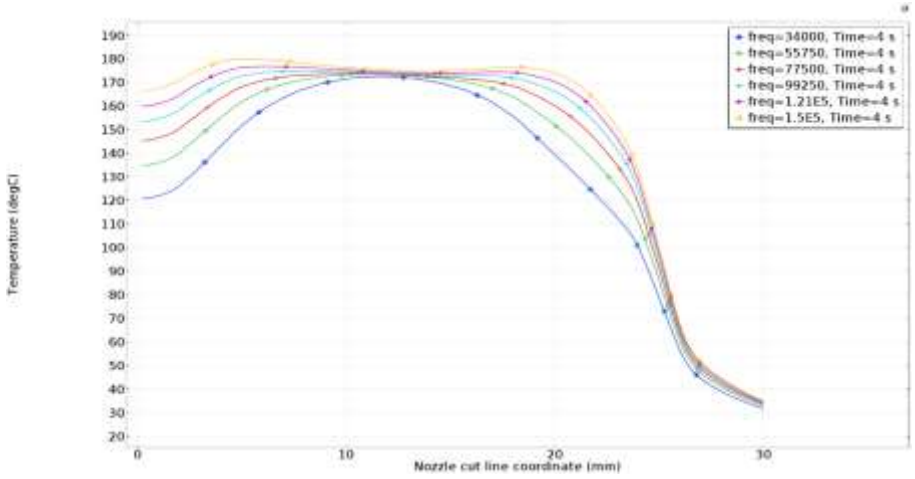

Figure 8 Solution of thermal part of the parametric multi-physical task at f = 34.. 150 kHz, $\alpha = 1^{o}$

On the basis of the data presented in Fig. 8 we can conclude that the completed optimization practically linearise the temperature curve for the major part of the area characterized by active heating of the nozzle. Maximum linearity of the parameters is provided at a frequency of approximately f = 121 kHz. The temperature variation of such

heating parameters is not more than 10° C, which is a very good result. To compare the heating evenness before and after the optimization, please refer to the temperature curves for the original values of f, t, and α as well as for their optimal values presented in one Figure.

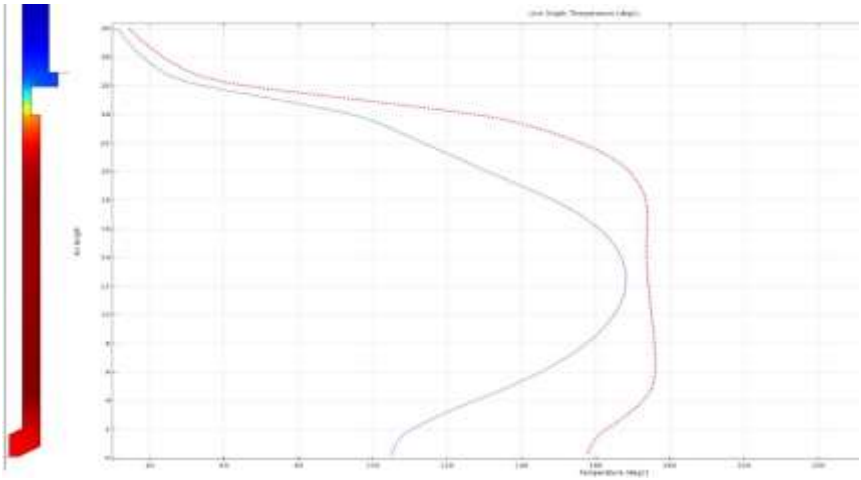

Figure 9 Consolidated graph of temperature distribution at f = 19.5 kHz, α = 0 (blue) and f = 121kGc, α = 0 (red). Heating time t = 4 s

It is worth noting that the optimized option is characterized by a much more rapid temperature change in the thermal barrier area, which results in the reduction of the transition zone height from 10 mm to almost the height of the thermal barrier (2 mm), which is an extremely high result.

3. EXPERIMENTAL CONFIRMATION OF THE MODELLING RESULTS

To confirm the results of the completed numerical modelling the authors designed a test stand, which comprises laboratory power supplies with U = 24V, Imax = 5A, DRV8302-based power controller, back end with MOSFET transistors, and Control Board based on ARM-micro controller STM32F334R8 by STMicroelectronics. Rated values of elements in LLC-resonance circuit were converted to fit the operating frequency of f = 121.3 kHz. The modified inductor was formed with 20 coils of copper litz wire (d = 1.2 mm, 2 layers). The geometry of the induction extruder complies with the one shown in Fig. 7. The appearance of the pilot extruder as well as the ferromagnetic nozzle are shown in Fig. 10, 11.

Figure 10 Appearance of pilot extruder

Figure 11 Appearance of ferromagnetic nozzle

The induction extruder was mounted on a 3D printer, whereupon a number of copies of a test product (parallelepiped with a base of 30 x 30 mm and height of 5 mm) were printed using various types of plastic. The printing output is shown in Fig. 12.

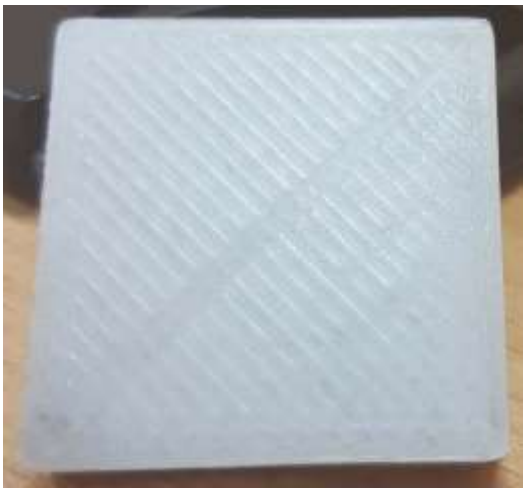

Figure 12 Appearance of the test product surface printed of nylon

It is worth noting that the polymer (nylon) shown in the photo is characterized by a large 'spurious' efflux from the work nozzle opening when heated. Nevertheless, being fed with this plastic, the experimental extruder demonstrates successful printing without any visible defects.

The results of the completed experiment showed a significant increase in printing quality (absence of spurious plastic efflux, absence of overheated areas with temperature-driven changes in filament colour), as well as an increase of the extruder nozzle heating rate (from room to operating temperature) by 35%.

4. CONCLUSIONS

The completed modelling revealed considerable unevenness of the extruder nozzle heating (76 °C), which significantly impacts the final quality of 3D printing products. Two main reasons of the observed quality reduction due to the uneven heating were described. The modelling results are confirmed by the experimental data obtained with the original sample of the induction extruder.

- - The next stage of modelling, which was to solve the parametric task, allowed to determine optimal frequency of the induction heating: (f) = 121.3 kHz. This frequency provides for the maximum evenness of the temperature curve that describes the extruder nozzle heating process.

- - In order to eliminate the residual unevenness, the authors proposed an approach based on changing the geometric shape of the inductor by inclining its coiling base. To determine the optimal angle, an additional parametric task was solved.
- - The completed analysis with the view to the identified optimal parameters of f = 121.3 kHz, $\alpha = 1^0$ showed dramatic reduction of the heating unevenness (from 76 to 10 °C). The test stand designed to confirm the results of the simulation modelling showed a significant increase in print quality (absence of spurious efflux of plastic, absence of overheated areas with temperature-driven changes in filament colour), as well as an increase in the rate of extruder heating from room to operating temperature by 35%.

ACKNOWLEDGEMENTS

The reported study was partially supported by the Government of Perm Krai research project Nr. S-26/795 of December 21, 2017 (the mathematical formulation), by the grants from the Russian Foundation for Basic Research RFBR Nr. 18-08-01016 A (the mathematical formulation electromagnetic task.), as well as by Ministry of Education and Science of the Russian Federation at the base part of the state assignment Nr. 9.9697.2017/BCh (Experimental confirmation of the modelling results).

REFERENCES

[1] Chennakesava, P. and Narayan, Y. S. Fused deposition modeling-insights. *International Conference on Advances in Design and Manufacturing (ICAD&M'14)*, pp. 1345-1350.

[2] Grimm, T. et al. Fused deposition modelling: a technology evaluation. Time-compression technologies, 11(2), 2003, pp.1-6.

[3] Simpson, P. G. *Induction heating: coil and system design*. McGraw-Hill, 1960.

[4] Bukhanov, V. M., Glushkova, T. M., Matynin, A. V., Saletskiy, A. M. and Kharabadze, D. E. SKIN-EFFEKT [Skin Effect]. Moscow, 2011.

[5] Stirling, R. L., Chilson, L., English, A. Inductively heated extruder heater: Patent 9596720 USA. – 2017. (Stirling, Ralph L., Luke Chilson, and Alex English. "Inductively heated extruder heater." U.S. Patent No. 9,596,720. 14 Mar. 2017.)

[6] Cai, Y. Instinctive Computing. Springer, 2017, pp. 112-113.

[7] Hofstaetter, T. et al. Simulation of a downsized FDM nozzle. *COMSOL Conference 2015*.

[8] Irodov, I. E. *Osnovnye zakony elektromagnetizma* [Basic principles of electromagnetics] students book for higher educational institutions - 2nd, stereotype. Moscow: Vysshaya Shkola, 1991.

[9] Comsol, A. B. AC/DC Module–User's Guide. COMSOL, 3, 2011, p. 151.

[10] Podoltsev, A. D. and Kucheryavaya, I. N. *Elementy teorii i chislennogo rascheta elektromagnitnykh protsessov v provodyashchikh sredakh* [The elements of theory and numerical simulation of electromagnetic processes in conducting media], Kiev: Institut Electrodinamiki, Natsionalnoi Academii Nauk Ukrainy, 1999.

[11] Slukhotsky, A. E. and Ryskin, S. E. *Inductory dlya induktsionnogo nagreva* [Inductors for induction heating]. Leningrad: Energiya, 1974.

[12] Shidlovsky, A. K., Shcherba, À. À., Podoltsev, A. D., Kucheriavaya, I. N. and Zolotarev, V. M. Induction heating of segmental wire conductor (Milliken type conductor) of power cable at manufacturing stage. *Tekhnichna electrodinamika*, 1, 2009, pp. 53-60.

[13] Hameyer, K., Driesen, J., De Gersem, H. and Belmans, R. The classification of coupled field problems. *IEEE Transactions on Magnetics*, 35(3), 1999, pp. 1618-1621.

[14] Kumbhar, G. B., Kulkarni, S. V., Escarela-Perez, R. and Campero-Littlewood, E. Applications of coupled field formulations to electrical machinery. *The International Journal for Computation and Mathematics in Electrical and Electronic Engineering (COMPEL)*, 26(2), 2007, pp. 489-523.